Article
Vol. 26, No. 5, p. 637–647, October 2022
https://doi.org/10.1007/s12303-022-0009-y
pISSN 1226-4806 eISSN 1598-7477
Geosciences Journal GJ

An optimal strategy for determining triple oxygen isotope ratios in natural water using a commercial cavity ring-down spectrometer

Songyi Kim[1,2], Changhee Han[1], Jangil Moon[1], Yeongcheol Han[1]*, Soon Do Hur[1], and Jeonghoon Lee[2]

[1]Korea Polar Research Institute, Incheon 21990, Republic of Korea
[2]Department of Science Education, Ewha Womans University, Seoul 03760, Republic of Korea

ABSTRACT: Triple oxygen isotope ratios have been increasingly acknowledged as useful hydrological tracers but measuring both $^{17}O/^{16}O$ and $^{18}O/^{16}O$ ratios with meaningful precision has been challenging due to the much lower natural abundance of ^{17}O than ^{16}O and even ^{18}O. In this study, in line with the advancement of laser-based techniques and their growing applications, we demonstrate how to optimize the determination of ^{17}O-excess ($\Delta^{17}O = \ln(\delta^{17}O + 1) - 0.528 \times \ln(\delta^{18}O + 1)$) in natural water using a commercial wavelength-scanned cavity ring-down spectrometer (WS-CRDS). We particularly focus on how to decide the injection numbers of samples and standard solutions utilized for normalization of sample results to the VSMOW-SLAP reference scale. With a measurement strategy aimed at an uncertainty better than 10 per meg (1σ), the $\Delta^{17}O$ of Greenland Ice Sheet Precipitation (GISP) is determined to be 24 ± 9 per meg (n = 104), in agreement with previous literature values. By applying this method to Antarctic glacial ice, it is shown to be useful in detecting the seasonality of $\Delta^{17}O$ values in Antarctic precipitation. Our approach represents an underlying analytical method that provides guidelines for determining $\Delta^{17}O$ from various types of natural waters.

Key words: triple oxygen isotopes, CRDS, $\delta^{17}O$, ^{17}O-excess, Antarctica snow

Manuscript received November 18, 2021; Manuscript accepted April 20, 2022

1. INTRODUCTION

Advances in laser spectrometry techniques have lowered the barrier to entry for precise measurements of triple oxygen isotope ratios ($\delta^{17}O$ and $\delta^{18}O$, where $\delta^{i}O = (^{i}O/^{16}O)_{sample}/(^{i}O/^{16}O)_{standard} - 1$) in water for potential applications in atmospheric, hydrologic, and paleoclimatic studies utilizing mass-dependent deviations between $\delta^{17}O$ and $\delta^{18}O$ as a complementary tool for understanding water cycles (Gat, 1996; Angert et al., 2004; Farquhar et al., 2007; Luz and Barkan, 2010; Uemura et al., 2010; Aron et al., 2021; Nyamgerel et al., 2021). The isotopic compositions of meteoric water are shown to form a linear trend in a plot of $\ln(\delta^{17}O + 1)$ vs. $\ln(\delta^{18}O + 1)$ with a slope of 0.528 (Meijer and Li, 1998; Barkan and Luz, 2005), and this is referred to as the global meteoric water line (GMWL) of the triple oxygen isotopes (Luz and Barkan, 2010). A deviation of $\delta^{17}O$ from the GMWL, expressed by ^{17}O-excess ($\Delta^{17}O = \ln(\delta^{17}O + 1) - 0.528 \times \ln(\delta^{18}O + 1)$), has been employed as a secondary isotope parameter that characterizes target water with triple oxygen isotopes and contributes to quantitatively distinguishing kinetic and equilibrium fractionation imprinted in target water (Barkan and Luz, 2007).

Due to its small natural variability, $\Delta^{17}O$ is expressed in per meg (10^{-6}) (Gat, 1996), while $\delta^{18}O$, $\delta^{2}H$ ($\delta^{2}H = (^{2}H/^{1}H)_{sample}/(^{2}H/^{1}H)_{standard} - 1$) and d-excess (deuterium excess; DE = $\delta^{2}H - 8 \times \delta^{18}O$) are typically reported in units of per mil (10^{-3}). Previously, commercial laser absorption spectrometers have achieved sufficient precision and accuracy to detect variations in $\Delta^{17}O$ in natural water (Berman et al., 2013; Steig et al., 2014). In addition to performance comparable to that of conventional isotope ratio mass spectrometry (IRMS), the laser-based technique has the advantage of simultaneous measurements of $\delta^{17}O$, $\delta^{18}O$ and $\delta^{2}H$ directly on vaporized water with relatively simple sample pretreatments. Two commercial analyzers have been used for the high-precision $\Delta^{17}O$ measurement: CRDS (cavity ring down spectroscopy, Picarro, USA) and OA-ICOS (off-axis integrated

---

***Corresponding author:**
Yeongcheol Han
Korea Polar Research Institute, 26 Songdomirae-ro, Yeonsu-gu, Incheon 21990, Republic of Korea
Tel: +82-32-760-5481, Fax: +82-32-760-5397, E-mail: yhan@kopri.re.kr

cavity output spectroscopy, Los Gatos Research Inc., USA) analyzers. Regardless of differences in their optical cavity designs, both analyzers are shown to be capable of attaining precision better than ~10 per meg (1σ) by increasing the signal-to-noise ratio by averaging signals (Berman et al., 2013; Steig et al., 2014). The optimal signal averaging times for both analyzers, as derived from Allan deviations, are several minutes (< 10^3 seconds) and are set as the factory defaults. For accuracy, instrumental outputs are typically scaled to two primary isotopic reference materials for water, VSMOW (Vienna Standard Mean Ocean Water) and SLAP (Standard Light Antarctic Precipitation). While VSMOW has δ^{17}O and δ^{18}O and hence Δ^{17}O of zero by definition, Δ^{17}O of SLAP is also considered zero with the consent of recent authors (e.g., Schoenemann et al., 2013 and references therein). As a consequence, inserting $\Delta^{17}O = 0$ and $\delta^{18}O = -55.50$‰ into the Δ^{17}O equation yields a δ^{17}O value of −29.6986 (as is given in Schoenemann et al., 2013). These isotopic ratios of the standards have been used to normalize the results of unknown samples to the VSMOW-SLAP scale; this normalization method is practically identical to conventional linear calibration.

In practice, achieving the best performance from a commercial Δ^{17}O analyzer is often challenging due to isotopic differences in water samples analyzed in succession. Despite purging with dry gas between sample injections, the residual water from an injection causes *memory effects* in the analysis of the subsequent injection. Several approaches have been applied to minimize memory effects. For example, memory effects can be mathematically corrected if they occur systematically (Pierchala et al., 2019; Vallet-Coulomb et al., 2021), but additional inspection should be made to determine whether the correction is appropriate. More simply, the first several injections made after switching samples can be excluded from the results, considering that those injections would suffer significant memory effects (Barkan and Luz, 2005; Penna et al., 2012; Gzquez et al., 2015). In this case, more injections are needed when the isotopic differences are larger across target waters (e.g., 55.5‰ for δ^{18}O between VSMOW2 and SLAP2), which adversely prolongs measurement time and reduces sample throughput. To eliminate memory effects, a duplicate vial containing the same solution is sometimes prepared and used for those extra injections (Wassenaar et al., 2014). Salt build-up inside the vaporizer due to repeated evaporation of impure water requires additional attention. The accumulating salts increase the surface area with which water vapor can interact, exacerbating memory effects over the analysis time (Skrzypek and Ford, 2014). Only regular removal of accumulated salts will reduce the memory effect in this case, and a mathematical correction or an increase in the number of injections is likely inappropriate. Organic materials in samples having water-like absorption features can directly interfere with measurement and cause memory effects if they remain in the vaporizer or cavity (Brand, 2010). Overall, the strategy used to overcome the memory effects can differ depending on the isotopic composition and purity of the water samples.

In this study, we present a practical method for optimal determination of Δ^{17}O in Antarctic ice using a Picarro L2140-*i* analyzer. Polar ice represents the purest natural water and hence causes the least salt buildup and minimal intersample memory effects, so it is an appropriate water type for evaluating analyzer performance and developing an underlying analytical method for various types of natural waters. We simulate measurement precision, which varies with the number of injections per vial, and the numbers and isotopic compositions of standard solutions utilized for VSMOW-SLAP normalization, by means of bootstrap approaches. The utility of the uncertainty simulation is verified by comparing the results with instrumental measurements. We report Δ^{17}O of GISP (Greenland Ice Sheet Precipitation) and compare the results with previous literature values. We also present the results of an in-house standard solution with an interlaboratory comparison. Finally, these simulations and instrumental experiments are applied to detect seasonal variations in Δ^{17}O in Antarctic ice cores.

2. METHODS

2.1. Instrumentation

An isotopic water analyzer (L2140-*i*, Picarro, USA), developed with the aim of providing precise and simultaneous measurements of δ^{17}O, δ^{18}O and δ^{2}H (Steig et al., 2014), was used. Here, we present a general overview of liquid water analyses using the L2140-i with the aid of commercial peripherals dedicated to automated discrete liquid sampling analyses, the A0325 autosampler and the A0211 vaporizer manufactured by Picarro, Inc.

Liquid samples were evaporated in the peripheral modules and introduced as water vapor into the optical cavity of the L2140-i. The autosampler operated a Hamiltonian syringe (part number 002980, SGE, Australia) to transfer ~1.8 μL water per injection from a 2 mL vial (part number 60180-508, Thermo Fisher Scientific, USA) to the vaporizer module. The vaporizer evaporated the allocated liquid water at 110 °C and mixed it with dry carrier gas (99.999% N_2 in this study) to give a final water vapor level of ~20,000 ppm. Then, the sample gas was delivered to the optical cavity in the analyzer, where a change in the ring-down time of the intensity of laser light due to absorption by water vapor was measured. With the interplay of the diaphragm vacuum pump, the position-controlled valve and the heating module, the gas flow across the optical cavity was kept at a constant rate (~40 sccm) under stabilized pressure (50 Torr) and temperature (80 °C).

Using the factory default for high precision Δ^{17}O measurements, the entire operation took approximately 9 minutes from one injection to the next. The built-in *coordinator* software yielded a single result per injection by integrating the output signals for ~260 seconds. Unless noted otherwise, all data presented in this study are based on the *coordinator* results.

2.2. Materials

As reference materials (RMs), VSMOW2, SLAP2 and GISP were used in this study. VSMOW2 and SLAP2, which replaced VSMOW and SLAP (Lin et al., 2010), respectively, were provided in sealed 20 mL glass ampoules by the International Atomic Energy Agency (IAEA, 2009). The GISP solution, also contained in a 20 ml glass ampoule, was purchased from the National Institute of Standards and Technology (NIST SRM 8536). We divided an ampoule of RMs into 400 μL aliquots in vial inserts placed in 2 ml glass vials. Each vial was weighed to ensure no water loss during storage (< 4 months maximum). All glassware and plasticware were dried in an oven at 50 °C for at least 24 hours before use. The isotopic compositions (δ^{17}O, δ^{18}O, and δ^{2}H) of the RMs used in this study are 0, 0, and 0‰ for VSMOW2, −29.6986, −55.50, and −427.5‰ for SLAP2, and −13.10, −24.72, and −189.5‰ for GISP (Table 1).

An in-house standard solution (STYX) was prepared by melting ~20 kg of firn cores drilled on the Styx glacier in Northern Victoria Land, Antarctica (73°54′S, 163°46′E, 1,750 m asl). The meltwater was filtered through a 0.45 μm nylon filter, divided into 20 ml glass ampoules and weighed after sealing. Each ampoule was weighed before opening to check for water loss and then treated the same as RMs. The STYX solution was used to verify normalization to the VSMOW-SLAP scale, to monitor instrumental drift and to evaluate the external reproducibility of measurements. The isotopic composition of STYX was determined from measurements performed over more than a year. Additionally, the STYX solution was sent to IsoLab at the University of Washington and analyzed independently by using CRDS (L2140-*i*) and dual-inlet IRMS (ThermoFinnigan MAT 253) with fluorination of water to O_2 (Steig et al., 2014).

The Antarctic ice samples were melted at room temperature and filtered through 0.45 μm syringe filters into 2 ml glass vials or inserted insets (400 μL) depending on sample availability. Ice cores obtained at the Antarctic GV7 site (70°41′17.1″S, 158° 51′48.9″E; 1950 m asl) during the 2013–2014 summer season were analyzed every 0.04 m for the depth interval of 3.9–8.1 m (n = 100) by following the measurement sequence presented in Table 2. The external reproducibilities (standard deviation, SD) for δ^{18}O and δ^{2}H were 0.05‰ and 0.4‰, respectively.

All solutions were prepared in a pair of vials subject to successive analyses. The vial analyzed first served as a buffer

Table 2. Configuration of the measurement sequence for Antarctic ice samples

Vial position	Solution	Number of injections (n_{inj})[(a)]
1	VSMOW2	15
2	VSMOW2	22
3	GISP	15
4	GISP	22
5	SLAP2	15
6	SLAP2	22
7	STYX	15
8	STYX	16
9–10	Sample #1	16
11–12	Sample #2	16
13–14	Sample #3	16
15–16	Sample #4	16
17–18	Sample #5	16
19	STYX	16
20	STYX	16
21–22	Sample #6	16
...	...	...

All solutions were prepared in a pair of vials (See Section 2.2).
[(a)] The last eight injections were used to evaluate the results for each solution.

Table 1. Water isotope compositions of the reference materials (RMs) used in this study

	δ^{17}O (‰)	δ^{18}O (‰)	Δ^{17}O (per meg)	δ^{2}H (‰)	DE (‰)[(a)]
Reference materials					
VSMOW2	0	0[(b)]	0	0[(b)]	0
SLAP2	−29.6986[(c)]	−55.50[(b)]	0	−427.5[(b)]	16.5
GISP	−13.10[(d)]	−24.72[(d)]	24[(d)]	−189.5	8.6
In-house standard[(e)]					
STYX	−18.44	−34.69	28	−272.3	5.2

[(a)] Calculated from δ^{18}O and δ^{2}H.
[(b)] IAEA (2009).
[(c)] Schoenemann et al. (2013).
[(d)] This study. See Section 3.3 and Table 5 for details.
[(e)] See Section 3.3 for details.

https://doi.org/10.1007/s12303-022-0009-y

against sample cross-contamination that may be caused by the autosampler syringe. It also helped in monitoring memory effects, especially when its isotopic compositions differed significantly from those of the previous sample. Otherwise, the results from both vials can be considered duplicates and combined to obtain better statistics through postprocessing.

2.3. Analytical Precision of the Instrument

An Antarctic ice meltwater sample was repeatedly injected 296 times over 45 hours to examine instrumental precision for $\Delta^{17}O$ determinations. The standard deviations (SDs) of $\delta^{17}O$ and $\delta^{18}O$ were 0.025‰ and 0.028‰, respectively. Instrumental drift was negligible over the analyses, and this was supported by the fact that no significant change was seen among randomly subsampled 10–100 consecutive injections out of the 296 injections (Fig. 1a). The measured SD for $\Delta^{17}O$ was 17 per meg, which is comparable to the manufacturer's specification (15 per meg). This precision is better than that estimated from the $\Delta^{17}O$ equation by uncertainty propagation (30 per meg). This is because the measured $\delta^{17}O$ and $\delta^{18}O$ values were correlated ($r = 0.78$) and had common sources of uncertainty cancelled out in the $\Delta^{17}O$ calculation.

The $\Delta^{17}O$ results were well described by a Gaussian distribution curve (Fig. 1b), and the *standard error of the mean* (SE) was improved to $17/\sqrt{n_{inj}}$ (Fig. 1c), suggesting that more accurate results can be obtained by increasing the number of injections (n_{inj}). Schauer et al. (2016) suggested that instrumental precision can be further improved by varying the signal averaging time for different isotope ratios, which requires an end user to access and analyze raw data recorded at a high rate (~1 Hz) instead of relying on the built-in *coordinator* software that yields a single result per injection. The types and structures of low-level data recorded at higher rates and methods for accessing them are described in Schauer et al. (2016). Nevertheless, we focus here on how to optimize $\Delta^{17}O$ analyses in natural water while insisting on using the *coordinator* software results that can be handled easily by end users.

2.4. Uncertainty Propagation Through VSMOW-SLAP Normalization

Measured values from the instrument are given in δ notation based on the predefined relationship between isotopic composition and analyzer response. This relationship should be regularly adjusted due to potential drift of instrumental conditions with time. Typically, to cope with instrumental drift, RMs are regularly analyzed along with samples and used to normalize the sample results. Measurements of both standards and samples are subject to uncertainties arising from instrumental precision (SD of 17 per meg), which jointly propagate to the final normalized result. Increasing n_{inj} for standards and samples may improve the uncertainty (SE; Fig. 1c) but lower throughput; n_{inj} is therefore to be optimally adjusted. In addition, the uncertainty in the final result can change with isotopic compositions and the numbers of standards used for VSMOW-SLAP normalization. To simulate these changes in uncertainty, we employed bootstrap approaches for 3 different cases (Table 3). The first case regarded VSMOW2 and SLAP2 as the standards and GISP as the sample. The second case examined changes seen in the uncertainty when the standards have smaller isotopic differences than the primary standards (VSMOW2 and SLAP2). This case represented an alternative use of secondary standard solutions (e.g., in-house standards) for VSMOW-SLAP normalization. The third case used VSMOW2, GISP and SLAP2 as standards and STYX as the sample, and the linear calibration method was used for normalization of the

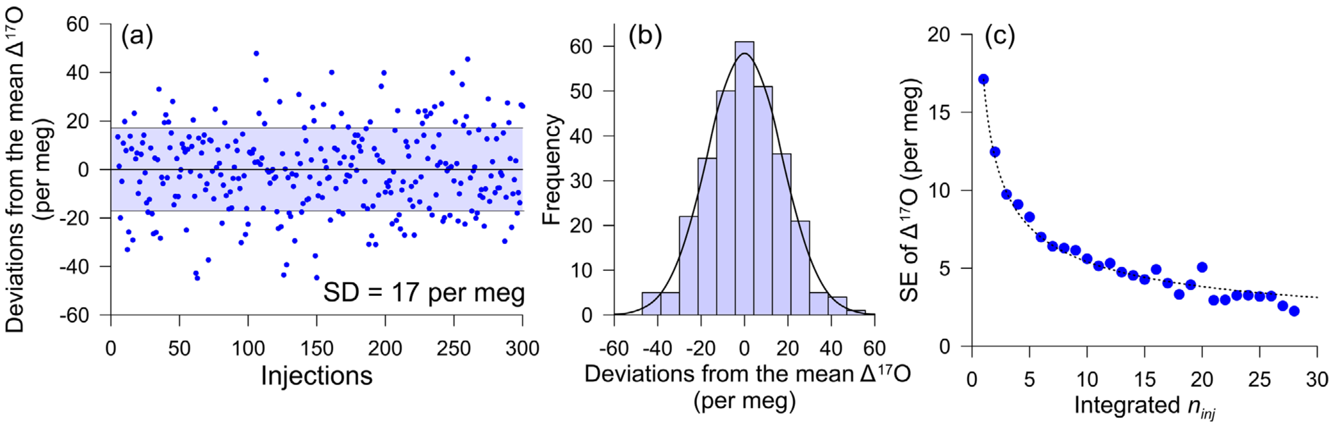

Fig. 1. (a) Deviations from the mean $\Delta^{17}O$ of repeated injections ($n = 296$) of an Antarctic snowmelt sample. The shaded area represents one standard deviation (SD = 17 per meg). (b) Histogram of (a). The solid line depicts the expected frequency from a Gaussian (normal) distribution with 1 SD of 17 per meg. (c) Changes in the standard error of the mean (SE) with the number of injections (n_{inj}) averaged. The dotted line depicts the expected SE from $17\sqrt{n_{inj}}$.

Table 3. Parameters of bootstrap approaches for uncertainty simulations

Parameters	Case 1	Case 2[a]	Case 3
Standards	VSMOW2, SLAP2	S1 ($\delta^{17}O = -10.60‰$, $\delta^{18}O = -20.00‰$, $\Delta^{17}O$ = 10 per meg), S2 ($\delta^{17}O = -18.87‰$, $\delta^{18}O = -35.50‰$, $\Delta^{17}O$ = 30 per meg)	VSMOW2, GISP, SLAP2
Sample	GISP	GISP	STYX
Number of injections (n_{inj})	From 2 to 21 for both standards and samples		
Repetition	> 40,000 for each n_{inj}		

[a] S1 and S2 are arbitrary standard waters with smaller isotopic differences than VSMOW2 and SLAP2.

sample results. This case was intended to examine the use of more standard solutions for VSMOW-SLAP normalization. For individual cases, the number of injections of the standards ($n_{inj,Std}$) and the sample ($n_{inj,Smp}$) varied from 2 to 21 (20×20 array), respectively.

The details of the uncertainty simulations are as follows. First, averages were eliminated from the $\delta^{17}O$ and $\delta^{18}O$ time series of the instrumental precision data (n = 296; Fig. 1) to obtain deviation time series. Then, for each combination of $n_{inj,Std}$ and $n_{inj,Smp}$, successive n_{inj} records were randomly resampled for each standard and sample from the deviation time series and added to the given isotopic compositions of the standards and the sample (Tables 1 and 3). The resampling-based $\delta^{17}O$ and $\delta^{8}O$ values were individually averaged, and the mean $\delta^{17}O$ and $\delta^{18}O$ values of the samples were normalized with those of the standards. Finally, the sample $\Delta^{17}O$ was calculated from the normalized $\delta^{17}O$ and $\delta^{18}O$ values. This series of calculations was repeated more than 40,000 times for each ($n_{inj,Std}$, $n_{inj,Smp}$) to evaluate the external reproducibility of the final normalized result.

2.5. Memory Effects

All surfaces that contact and interact with sample water during delivery from a vial to the optical cavity can act as sources of memory effects. The memory effects can increase the errors in the results and hence must be carefully assessed, especially when samples with large isotopic differences are analyzed in succession. In general, repeated injections of the same sample gradually reduce memory effects, which probably indicates that the sample contacting surfaces gradually reach equilibrium with the sample vapor and do not alter its isotope composition. In this study, we analyzed the memory effects occurring across RMs with large isotopic differences (> 20‰ for $\delta^{18}O$). We particularly focused on GISP and STYX, which were analyzed after RMs that were relatively enriched (VSMOW2) and depleted (SLAP2) in heavy isotopes, respectively (Table 2).

The extra injections used to relieve memory effects increased the total analysis time. Since those injections were excluded from the evaluation of results, a long signal integration time (~260 seconds per injection) for each of them may be unnecessary and could be shortened to increase sample throughput. We made slight modifications to the original scripts written in Python that controlled the signal integration time (Table 4). The signal integration times for the 1st, 3rd, 5th, and 7th injections from a sample vial were set to 0, which means that the liquid evaporated in the vaporizer but was exhausted without being transferred to the cavity. For the 2nd, 4th, and 6th injections, signal integration times were reduced to ~4 minutes. The consequent changes in measurement performance were investigated by comparing the results for GISP with those measured with the original scripts.

Table 4. Reduction of the signal integration time for injections from the 1st to the 7th

Injection from a vial	Signal integration time (minutes)
1st	0
2nd	~4
3rd	0
4th	~4
5th	0
6th	~4
7th	0
8th	~9
9th	~9
...	...

A zero means that the injected sample is evaporated in the vaporizer but exhausted without measurement. The original signal integration times were evenly ~9 minutes.

3. RESULTS AND DISCUSSION

3.1. Measurement Uncertainty

Uncertainty simulations can help to determine the value of n_{inj} required to achieve the desired precision in the measurements. For example, when using VSMOW2 and SLAP2 as standards (Case 1), at least 5 injections were necessary for both the standards and samples to attain a precision of < 10 per meg in the final normalized results (Fig. 2a). We note that this n_{inj}

https://doi.org/10.1007/s12303-022-0009-y

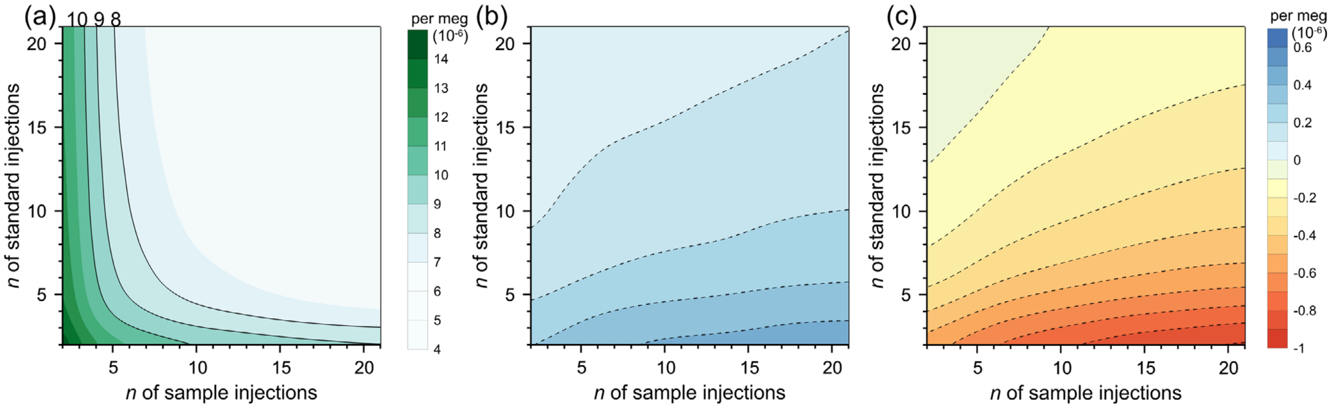

Fig. 2. (a) Expected external reproducibility of normalized sample results with varying n_{inj} of the two standards (VSMOW2 and SLAP2) and a sample (GISP) for Δ^{17}O. Uncertainty changes with the use of (b) standards having narrower isotope ratio ranges and (c) an additional standard are shown as differences from the first case.

indicates the number of injections to be averaged and does not include preceding extra injections used to overcome memory effects; therefore, the total number of injections shall be higher.

The simulated uncertainties for the three different cases are compared in Figure 2. While increasing n_{inj} commonly improves uncertainty, there were differences in the results for these cases. The use of standard solutions with smaller isotopic differences increased the uncertainty slightly, which was noticeable when n_{inj} was large for the sample and small for the standards (Case 2 – Case 1 < 0.6 per meg; Fig. 2b). In other words, when secondary standards with smaller isotopic differences were used, larger n_{inj} values were required to achieve uncertainties comparable to those seen when using the primary standards (i.e., VSMOW2 and SLAP2). The results for Case 3 showed that using an additional standard for VSMOW-SLAP normalization improved the use uncertainty (Case 3 – Case 1 < −1.2 per meg; Fig. 2c). The improvement was more marked when n_{inj} was large for the sample and small for the standards. If the comparisons are taken together, the use of the primary RMs (VSMOW2 and SLAP2) with additional RMs having intermediate isotopic compositions between those of the primary RMs was the most effective way to reduce the uncertainty of the Δ^{17}O measurement. Adding secondary RMs with intermediate isotopic compositions has the additional advantage of mitigating the memory effects between primary RMs caused by their large isotopic differences.

3.2. GISP and the In-house Standard (STYX)

The memory effects caused by the analyses of VSMOW2 and SLAP2 were imprinted in the following GISP and STYX analyses, respectively (Fig. 3). These cases represent the most extreme memory effects seen in this study, and they stemmed from the largest differences in isotope ratios between RMs (> 20‰ for δ^{18}O). The memory effects of VSMOW2 relatively enriched in ^{18}O increased the δ^{18}O value of GISP in the early injections (Fig. 3a). In contrast, those of SLAP2 relatively depleted in ^{18}O lowered δ^{18}O in the early injections of STYX. In both cases, the memory effects gradually disappeared with repeated injections but were not fully eliminated during measurement of the first vial of a pair of vials; they became unnoticeable after ~20 injections (< 0.04 of SD; Fig. 3). Memory effects were not identified in the results for Δ^{17}O, perhaps because the difference in Δ^{17}O values for the solutions was too small (< 30 per meg).

Figure 3a compares the results for GISP with (red closed squares) and without (blue open circles) reducing the signal integration times for early injections. Since Figure 3 contains only the results of measured injections, there was an additional injection made before each of the initial four injections in the experiment with the shortened signal integration (Table 4), which evaporated in the vaporizer but was not measured. The comparison shows that the shortened signal integration was sufficient to eliminate the memory effects and made little difference in the results after ~20 measured injections. Therefore, increasing the injection number without measurements could be a practical way to enhance sample throughput. This will also help to minimize potential sample evaporation from vials once punctured by autosampler syringes. However, this approach is recommended only for highly pure water samples since increasing injections of impure water will cause more salts to accumulate in the vaporizer and worsen the memory effects. Again, memory effects should be dealt with differently depending on sample conditions. We note that, in practice, memory effects can be further aggravated by mechanical factors such as an aged autosampler syringe, an inappropriately adjusted syringe plunger, a vial overpressured by the water sample, or aged diaphragms in the vacuum pump for the vaporizer.

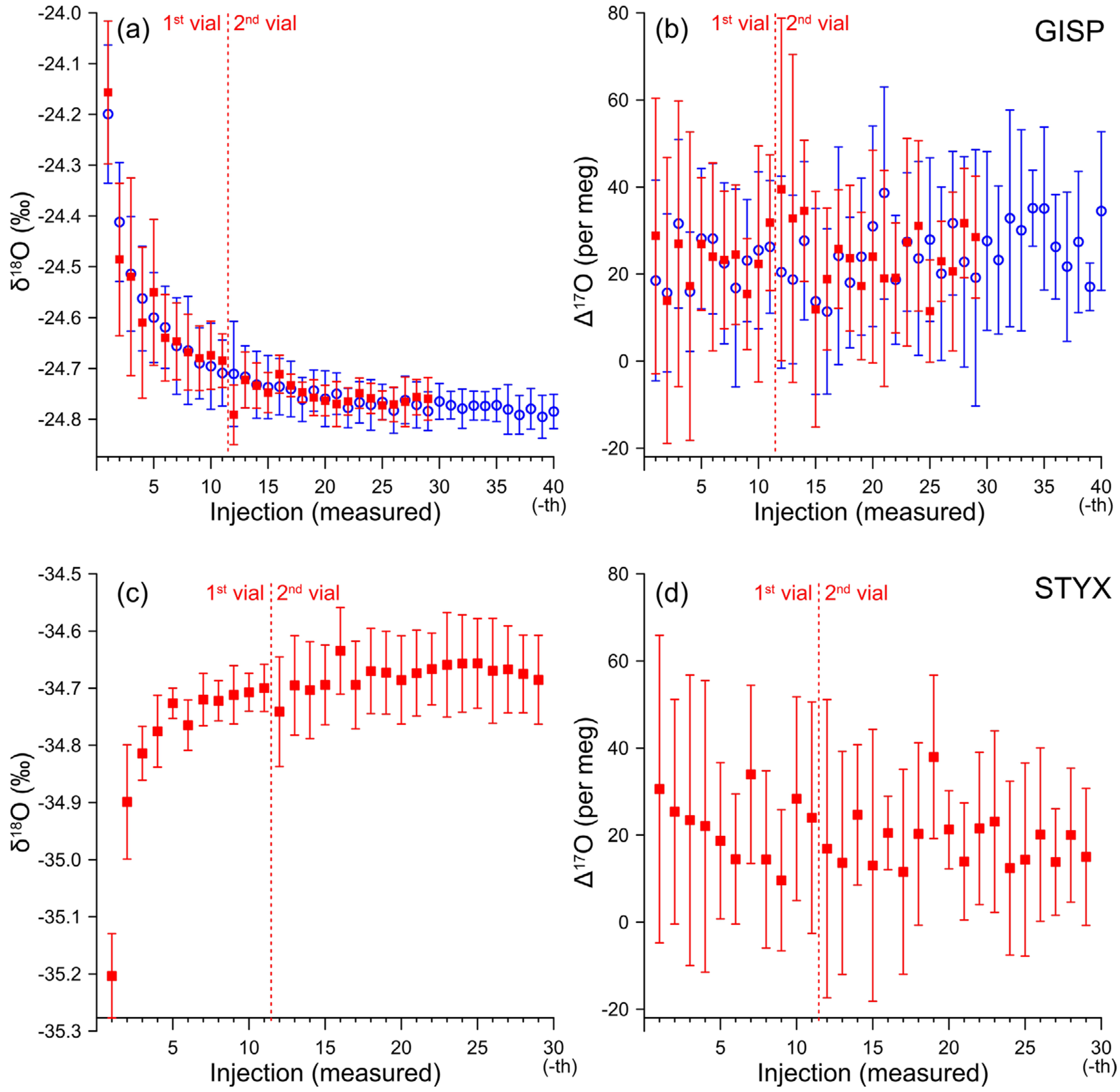

Fig. 3. Variations in (a) $\delta^{18}O$ and (b) $\Delta^{17}O$ of GISP injected after VSMOW2 and analyzed with (red square; Table 4) and without (blue dot) reductions of signal integration time for early injections. (c and d) Variations in $\delta^{18}O$ and $\Delta^{17}O$ for STYX injected after the SLAP2 analysis.

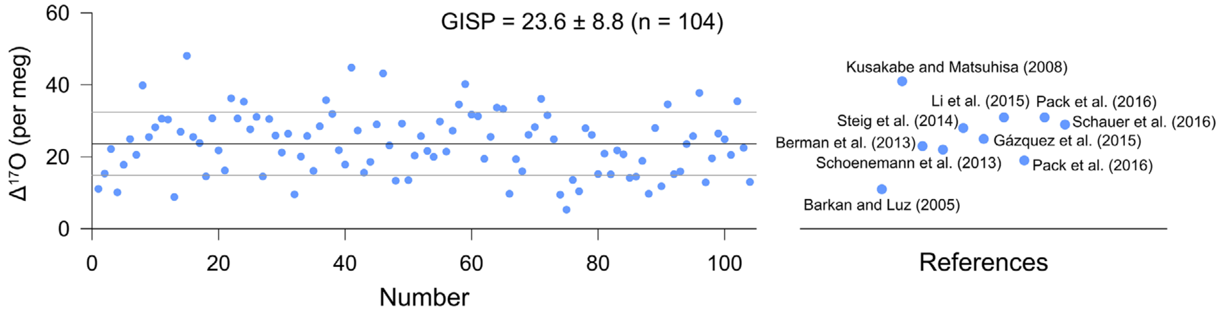

Fig. 4. Long-term reproducibility for measurements of GISP with comparisons to the literature values.

Figure 4 shows long-term $\Delta^{17}O$ measurements of GISP performed over 12 months with comparisons to the literature values. The mean $\Delta^{17}O$ was determined to be 24 ± 9 (SD, n = 104) per meg and agreed with previous results (Table 5).

The in-house STYX solution analyzed over the same period had a mean $\Delta^{17}O$ of 28 ± 9 per meg (n = 180) with external reproducibility comparable to that of the GISP results. The results for STYX determined at IsoLab (University of Washington)

Table 5. Triple oxygen isotope compositions of GISP obtained in this and previous studies

$\delta^{17}O$ (‰)	$\delta^{18}O$ (‰)	$\Delta^{17}O$ (per meg)	Reference
VSMOW-SLAP scale			
−13.10 (0.05)$^{(a)}$	−24.72 (0.09)	24 (9)	This study
−13.11	−24.80	70$^{(b)}$, 41$^{(c)}$	Kusakabe and Matsuhisa (2008)
−13.12 (0.05)	−24.74 (0.07)	23 (10)	Berman et al. (2013)
−13.16 (0.05)	−24.82 (0.08)	22 (11)	Schoenemann et al. (2013)
−13.1444	−24.80 (0.02)	28 (2)	Steig et al. (2014)
−13.09$^{(a)}$	−24.7 (0.2)	31 (11)	Li et al. (2015)
−13.188 (0.042)	−24.866 (0.082)	19 (4)	Pack et al. (2016)
−13.016 (0.184)	−24.566 (0.335)	31 (7)	Pack et al. (2016)
−13.1219 (0.04)	−24.76 (0.07)	29 (8)	Schauer et al. (2016)
VSMOW scale			
−13.12 (0.01)	−24.73 (0.2)	11$^{(c)}$	Barkan and Luz (2005)
–	–	25 (12)	Gázquez et al. (2015)

(a) 1σ uncertainty in parentheses.
(b) A GMWL slope of 0.5282 was used for the $\Delta^{17}O$ calculation.
(c) Schoenemann et al. (2013).

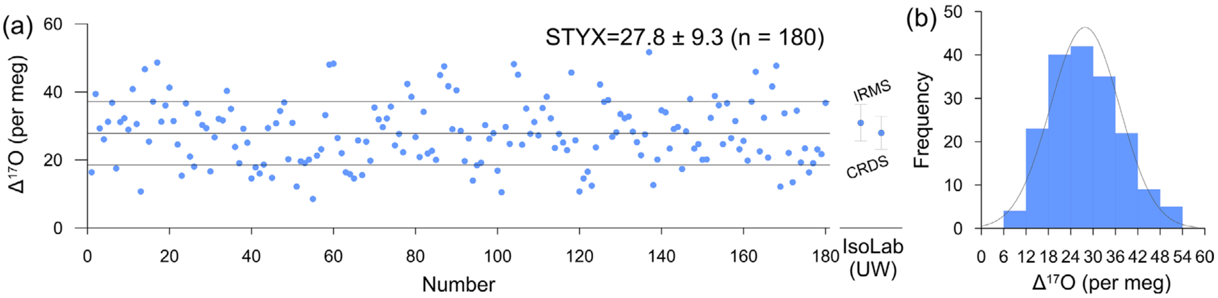

Fig. 5. (a) Long-term reproducibility for measurements of the in-house standard STYX with (b) a histogram of the results. The results of the interlaboratory comparison validate the accuracy of the measurements.

were 31 ± 5 per meg (n = 12; IRMS) and 28 ± 5 per meg (n = 15; CRDS), which were well matched to our results (Fig. 5a). These consistent results showed the possibility for further utilization of the STYX solution for VSMOW-SLAP normalization to improve the uncertainty of $\Delta^{17}O$ measurements.

The results of GISP and STYX were evaluated by averaging the last eight injections (Table 2), and their external reproducibilities (8.8 and 9.3 per meg; Figs. 4 and 5) were comparable to those expected from the uncertainty simulations (7.5 per meg when $n_{inj,Std} = n_{inj,Smp} = 8$; Fig. 2a). It could then be inferred that uncertainties in the external reproducibilities were dominated by the instrumental precision and memory effects from the VSMOW2 and SLAP2 were properly minimized. The slightly higher measured uncertainty than the simulated uncertainty might be due to other reasons, such as wear of consumable components (e.g., autosampler syringes, vaporizer septa, and diaphragms in vacuum pumps), N_2 gas supply stability, or human errors in handling small amounts of solutions. Normalizing the results of STYX using GISP as an additional standard solution improves the external reproducibility to 9.0 per meg. This improvement is consistent with what is expected from the uncertainty simulation (Case 3 – Case 1 = 0.3 per meg for $n_{inj,Std} = n_{inj,Smp} = 8$; Fig. 2c).

3.3. Natural Antarctic Ice Samples

Figure 6a shows $\Delta^{17}O$, $\delta^{18}O$, $\delta^{17}O$, $\delta^{2}H$ and d-excess for Antarctic GV7 ice core samples. The measured $\Delta^{17}O$ ranged from −10 to 70 per meg, with an average of 29 per meg (n = 100; Fig. 6a). The variability was comparable to those for precipitation and ice cores from the Antarctic Vostok station (−30–30 per meg; Landais et al., 2012a), precipitation at Dome C (−20–60 per meg; Touzeau et al., 2016) and Greenland ice cores (30–80 per meg; Landais et al., 2012b). The magnitude was also similar to the spatial variability of $\Delta^{17}O$ along several East Antarctic transects (Pang et al., 2015; Touzeau et al., 2016).

The triple oxygen isotope compositions of the ice samples were best explained by the linear equation $\ln(\delta^{17}O + 1) = (0.5236 \pm 0.0007) \ln(\delta^{18}O + 1) - (0.00010 \pm 0.00002)$ (±1 SD; Fig. 6b). The slope was slightly smaller than that of the GMWL (0.528; Luz

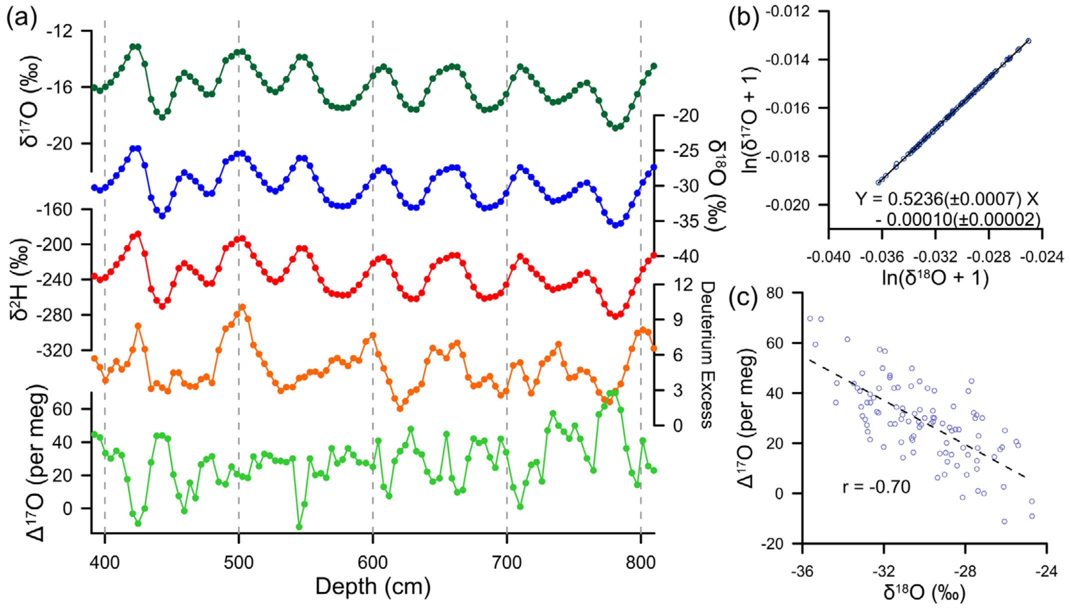

Fig. 6. (a) Variations in $\delta^{17}O$, $\delta^{18}O$, $\delta^{2}H$, DE and $\Delta^{17}O$ of GV7 ice cores for the depth interval 3.9–8.1 m. Plot of (b) $\ln(\delta^{17}O + 1)$ vs. $\ln(\delta^{18}O + 1)$ and (c) $\Delta^{17}O$ vs. $\delta^{18}O$.

and Barkan, 2010) but consistent with previous results for precipitation and snowpack from Vostok and Dome C (Touzeau et al., 2016), ice core samples with $\ln(\delta^{18}O + 1) > -37‰$ from the WAIS Divide (Schoenemann et al., 2014), and shallow ice cores from NEEM (Landais et al., 2012b). These slopes smaller than 0.528 may be due to the same cause as the seasonality of $\Delta^{17}O$ to be discussed below.

As with other water isotopic parameters, the seasonal variations in $\Delta^{17}O$ were clearly discernible. However, whereas $\delta^{17}O$, $\delta^{18}O$, $\delta^{2}H$, and DE are generally high in summer and low in winter, $\Delta^{17}O$ is low in summer and high in winter. Consequently, a negative correlation existed between $\Delta^{17}O$ and $\delta^{18}O$ ($r = -0.70$; Fig. 6c). With insufficient measurement data, the mechanism that brings seasonality to $\Delta^{17}O$ for Antarctic ice is not yet fully understood. Previously, the negative relationship between $\Delta^{17}O$ and $\delta^{18}O$ in Antarctic ice was first reported for a Vostok surface snowpack, and ^{17}O-enriched stratospheric water was proposed as a possible source of higher $\Delta^{17}O$ in winter snow layers (Winkler et al., 2013). However, another study on precipitation at Vostok reported positive correlations between $\Delta^{17}O$ and $\delta^{18}O$ and suggested that they could be explained by temporal changes in the relative contributions of equilibrium and kinetic fractionation during condensation (Landais et al., 2012a). Miller (2018) proposed that the precipitation type (i.e., diamond dust vs. cloud-derived precipitation) is an important control on $\Delta^{17}O$, especially in areas with low snowfall. With simulations using an intermediate complexity model, Schoenemann and Steig (2016) suggested that the annual cycle of $\Delta^{17}O$ in Antarctic coastal precipitation at the WAIS (West Antarctic Ice Sheet) Divide, where $\Delta^{17}O$ is negatively correlated with $\delta^{18}O$, is strongly influenced by seasonal changes in humidity at the water vapor source and sea ice conditions along the moisture transport path. Since the GV7 site has a similar elevation (1,950 m above sea level), mean annual temperature (−32 °C), and accumulation rate (~24 cm (water equivalent) yr^{-1}; Caiazzo et al., 2017) as WAIS (1,766 m, −30 °C, and ~22 cm yr^{-1}, respectively), it could be expected that the negative correlation between $\Delta^{17}O$ and $\delta^{18}O$ at GV7 occurred from the same causes. Due to relatively high snow accumulation compared to the inland plateau, the impact of stratospheric water vapor or diamond dust would be ignored. Indeed, the air mass back trajectory analysis at GV7 indicated the Western Pacific Ocean (WPO) as the major moisture source (~60%) without any apparent seasonality (Caiazzo et al., 2017). Then the seasonal changes in humidity in the WPO and sea ice conditions along the moisture transport paths might be key controls of the seasonality of $\Delta^{17}O$ at GV7. Comparisons with observational or reanalysis data and water isotope-enabled simulations will be helpful to develop quantitative explanations in future studies.

4. CONCLUSIONS

Based on the instrumental stability of commercial $\Delta^{17}O$ analyzers, we determined a way to make compromise decisions regarding appropriate numbers for injections of samples and RMs, taking into account the precision desired for the result and the sample throughput. Memory effects should also be considered, which usually increase the injection numbers. Uncertainty simulations and experiments suggested that averaging the results

https://doi.org/10.1007/s12303-022-0009-y

of 8 injections was sufficient to achieve reproducibility better than 10 per meg (1 SD) for a VSMOW-SLAP normalized result. However, up to 20 extra injections were required to overcome memory effects, especially when successively analyzed solutions had large differences in isotopic compositions, such as in the case of RMs. Arranging more RMs with isotope ratios between those of VSMOW2 and SLAP2 is recommended because it helps to mitigate memory effects across the analyses of RMs and improves measurement reproducibility. We prepared a pair of vials for each RM and natural sample to avoid memory effects in the results. However, unlike RMs, ice core samples, which are characterized by gradual changes in isotope compositions with depth, were found to be marginally affected by memory effects. It is therefore emphasized that strategies for dealing with memory effects can vary depending on sample characteristics. A shorter signal integration time for early injections, which are excluded from the results, may be an option for analyses of pure water.

ACKNOWLEDGMENTS

This study was supported by Korea Polar Research Institute (KOPRI) research grants (PE21440 and PE15150). The Antarctic GV7 ice cores were obtained through the IPICS-2kyr-It project, a PNRA (Italian Antarctic Research Programme) ice core project carried out in cooperation with KOPRI.

REFERENCES

Angert, A., Cappa, C.D., and DePaolo, D.J., 2004, Kinetic ^{17}O effects in the hydrologic cycle: indirect evidence and implications. Geochimica et Cosmochimica Acta, 68, 3487–3495. https://doi.org/10.1016/j.gca.2004.02.010

Aron, P.G., Levin, N.E., Beverly, E.J., Huth, T.E., Passey, B.H., Pelletier, E.M., Poulsen, C.J., Winkelstern, I.Z., and Yarian, D.A., 2021, Triple oxygen isotopes in the water cycle. Chemical Geology, 565, 120026. https://doi.org/10.1016/j.chemgeo.2020.120026

Barkan, E. and Luz, B., 2005, High precision measurements of $^{17}O/^{16}O$ and $^{18}O/^{16}O$ ratios in H_2O. Rapid Communications in Mass Spectrometry, 19, 3737–3742. https://doi.org/10.1002/rcm.2250

Barkan, E. and Luz, B., 2007, Diffusivity fractionations of $H_2{}^{16}O/H_2{}^{17}O$ and $H_2{}^{16}O/H_2{}^{18}O$ in air and their implications for isotope hydrology. Rapid Communications in Mass Spectrometry, 21, 2999–3005. https://doi.org/10.1002/rcm.3180

Berman, E.S.F., Levin, N.E., Landais, A., Li, S., and Owano, T., 2013, Measurement of $\delta^{18}O$, $\delta^{17}O$, and ^{17}O-excess in water by off-axis integrated cavity output spectroscopy and isotope ratio mass spectrometry. Analytical Chemistry, 85, 10392–10398. https://doi.org/10.1021/ac402366t

Brand, W.A., 2010, Comments on "Discrepancies between isotope ratio infrared spectroscopy and isotope ratio mass spectrometry for the stable isotope analysis of plant and soil waters". Rapid Communications in Mass Spectrometry, 24, 2687–2688. https://doi.org/10.1002/rcm.4685

Caiazzo, L., Baccolo, G., Barbante, C., Becagli, S., Bertò, M., Ciardini, V., Crotti, I., Delmonte, B., Dreossi, G., Frezzotti, M., Gabrieli, J., Giardi, F., Han, Y., Hong, S.-B., Hur, S.D., Hwang, H., Kang, J.-H., Narcisi, B., Proposito, M., Scarchilli, C., Selmo, E., Severi, M., Spolaor, A., Stenni, B., Traversi, R., and Udisti, R., 2017, Prominent features in isotopic, chemical and dust stratigraphies from coastal East Antarctic ice sheet (Eastern Wilkes Land). Chemosphere, 176, 273–287. https://doi.org/10.1016/j.chemosphere.2017.02.115

Farquhar, G.D., Cernusak, L.A., and Barnes, B., 2007, Heavy water fractionation during transpiration. Plant Physiology, 143, 11–18. https://doi.org/10.1104/pp.106.093278

Gat, J.R., 1996, Oxygen and hydrogen isotopes in the hydrologic cycle. Annual Review of Earth and Planetary Sciences, 24, 225–262. https://doi.org/10.1146/annurev.earth.24.1.225

Gázquez, F., Mather, I., Rolfe, J., Evans, N.P., Herwartz, D., Staubwasser, M., and Hodell, D.A., 2015, Simultaneous analysis of $^{17}O/^{16}O$, $^{18}O/^{16}O$ and $^{2}H/^{1}H$ of gypsum hydration water by cavity ring-down laser spectroscopy. Rapid Communications in Mass Spectrometry, 29, 1997–2006. https://doi.org/10.1002/rcm.7312

IAEA, 2009, Reference sheet for international measurement standards: VSMOW2 and SLAP2. International Atomic Energy Agency, Vienna.

Kusakabe, M. and Matsuhisa, Y., 2008, Oxygen three-isotope ratios of silicate reference materials determined by direct comparison with VSMOW-oxygen. Geochemical Journal, 42, 309–317. https://doi.org/10.2343/geochemj.42.309

Landais, A., Ekaykin, A., Barkan, E., Winkler, R., and Luz, B., 2012a, Seasonal variations of ^{17}O-excess and d-excess in snow precipitation at Vostok station, East Antarctica. Journal of Glaciology, 58, 725–733. https://doi.org/10.3189/2012JoG11J237

Landais, A., Steen-Larsen, H.C., Guillevic, M., Masson-Delmotte, V., Vinther, B., and Winkler, R., 2012b, Triple isotopic composition of oxygen in surface snow and water vapor at NEEM (Greenland). Geochimica et Cosmochimica Acta, 77, 304–316. https://doi.org/10.1016/j.gca.2011.11.022

Li, S., Levin, N.E., and Chesson, L.A., 2015, Continental scale variation in ^{17}O-excess of meteoric waters in the United States. Geochimica et Cosmochimica Acta, 164, 110–126. https://doi.org/10.1016/j.gca.2015.04.047

Lin, Y., Clayton, R.N., and Gröning, M., 2010, Calibration of $\delta^{17}O$ and $\delta^{18}O$ of international measurement standards – VSMOW, VSMOW2, SLAP, and SLAP2. Rapid Communications in Mass Spectrometry, 24, 773–776. https://doi.org/10.1002/rcm.4449

Luz, B. and Barkan, E., 2010, Variations of $^{17}O/^{16}O$ and $^{18}O/^{16}O$ in meteoric waters. Geochimica et Cosmochimica Acta, 74, 6276–6286. https://doi.org/10.1016/j.gca.2010.08.016

Meijer, H.A.J. and Li, W.J., 1998, The use of electrolysis for accurate $\delta^{17}O$ and $\delta^{18}O$ isotope measurements in water. Isotopes in Environmental and Health Studies, 34, 349–369. https://doi.org/10.1080/10256019808234072

Miller, M.F., 2018, Precipitation regime influence on oxygen triple-isotope distributions in Antarctic precipitation and ice cores. Earth and Planetary Science Letters, 481, 316–327. https://doi.org/10.1016/j.epsl.2017.10.035

Nyamgerel, Y., Han, Y., Kim, M., Koh, D.-C., and Lee, J., 2021, Review on applications of ^{17}O in hydrological cycle. Molecules, 26, 4468.

https://doi.org/10.3390/molecules26154468

Pack, A., Tanaka, R., Hering, M., Sengupta, S., Peters, S., and Nakamura, E., 2016, The oxygen isotope composition of San Carlos olivine on the VSMOW2-SLAP2 scale. Rapid Communications in Mass Spectrometry, 30, 1495–1504. https://doi.org/10.1002/rcm.7582

Pang, H., Hou, S., Landais, A., Masson-Delmotte, V., Prie, F., Steen-Larsen, H.C., Risi, C., Li, Y., Jouzel, J., Wang, Y., He, J., Minster, B., and Falourd, S., 2015, Spatial distribution of ^{17}O-excess in surface snow along a traverse from Zhongshan station to Dome A, East Antarctica. Earth and Planetary Science Letters, 414, 126–133. https://doi.org/10.1016/j.epsl.2015.01.014

Penna, D., Stenni, B., Šanda, M., Wrede, S., Bogaard, T.A., Michelini, M., Fischer, B.M.C., Gobbi, A., Mantese, N., Zuecco, G., Borga, M., Bonazza, M., Sobotková, M., Čejková, B., and Wassenaar, L.I., 2012, Technical note: evaluation of between-sample memory effects in the analysis of δ^2H and δ^{18}O of water samples measured by laser spectroscopes. Hydrology and Earth System Sciences, 16, 3925–3933. https://doi.org/10.5194/HESS-16-3925-2012

Pierchala, A., Rozanski, K., Dulinski, M., Gorczyca, Z., Marzec, M., and Czub, R., 2019, High-precision measurements of δ^2H, δ^{18}O and δ^{17}O in water with the aid of cavity ring-down laser spectroscopy. Isotopes Environmental and Health Studies, 55, 290–307. ?https://doi.org/10.1080/10256016.2019.1609959

Schauer, A.J., Schoenemann, S.W., and Steig, E.J., 2016, Routine high-precision analysis of triple water-isotope ratios using cavity ring-down spectroscopy. Rapid Communications in Mass Spectrometry, 30, 2059–2069. https://doi.org/10.1002/rcm.7682

Schoenemann, S.W., Schauer, A.J., and Steig, E.J., 2013, Measurement of SLAP2 and GISP δ^{17}O and proposed VSMOW-SLAP normalization for δ^{17}O and ^{17}O$_{\text{excess}}$. Rapid Communications in Mass Spectrometry, 27, 582–590. https://doi.org/10.1002/rcm.6486

Schoenemann, S.W., Steig, E.J., Ding, Q., Markle, B.R., and Schauer, A.J., 2014, Triple water-isotopologue record from WAIS Divide, Antarctica: controls on glacial-interglacial changes in ^{17}O$_{\text{excess}}$ of precipitation. Journal of Geophysical Research: Atmospheres, 119, 8741–8763. https://doi.org/10.1002/2014JD021770

Schoenemann, S.W. and Steig, E.J., 2016, Seasonal and spatial variations of ^{17}O excess and d excess in Antarctic precipitation: insights from an intermediate complexity isotope model. Journal of Geophysical Research: Atmospheres, 121, 11215–11247. https://doi.org/10.1002/2016JD025117

Skrzypek, G. and Ford, D., 2014, Stable isotope analysis of saline water samples on a cavity ring-down spectroscopy instrument. Environmental Science and Technology, 48, 2827–2834. https://doi.org/10.1021/es4049412

Steig, E.J., Gkinis, V., Schauer, A.J., Schoenemann, S.W., Samek, K., Hoffnagle, J., Dennis, K.J., and Tan, S.M., 2014, Calibrated high-precision ^{17}O-excess measurements using cavity ring-down spectroscopy with laser-current-tuned cavity resonance. Atmospheric Measurement Techniques, 7, 2421–2435. https://doi.org/10.5194/amt-7-2421-2014

Touzeau, A., Landais, A., Stenni, B., Uemura, R., Fukui, K., Fujita, S., Guilbaud, S., Ekaykin, A., Casado, M., Barkan, E., Luz, B., Magand, O., Teste, G., Le Meur, E., Baroni, M., Savarino, J., Bourgeois, I., and Risi, C., 2016, Acquisition of isotopic composition for surface snow in East Antarctica and the links to climatic parameters. The Cryosphere, 10, 837–852. https://doi.org/10.5194/tc-10-837-2016

Uemura, R., Barkan, E., Abe, O., and Luz, B., 2010, Triple isotope composition of oxygen in atmospheric water vapor. Geophysical Research Letters, 37. https://doi.org/10.1029/2009GL041960

Vallet-Coulomb, C., Couapel, M., and Sonzogni, C., 2021, Improving memory effect correction to achieve high precision analysis of δ^{17}O, δ^{18}O, δ^2H, ^{17}O-excess and d-excess in water using cavity ring-down laser spectroscopy. Rapid Communications in Mass Spectrometry 35, e9108. https://doi.org/10.1002/RCM.9108

Wassenaar, L.I., Coplen, T.B., and Aggarwal, P.K., 2014, Approaches for achieving long-term accuracy and precision of δ^{18}O and δ^2H for waters analyzed using laser absorption spectrometers. Environmental Science and Technology, 48, 1123–1131. https://doi.org/10.1021/es403354n

Winkler, R., Landais, A., Risi, C., Baroni, M., Ekaykin, A., Jouzel, J., Petit, J.R., Prie, F., Minster, B., and Falourd, S., 2013, Interannual variation of water isotopologues at Vostok indicates a contribution from stratospheric water vapor. Proceedings of the National Academy of Sciences of United States of America, 110, 17674–17679. https://doi.org/10.1073/pnas.1215209110